*Int. J. Electrochem. Sci.*, 12 **(2017)** 3965 – 3981, doi: 10.20964/2017.05.61

**International Journal of ELECTROCHEMICAL SCIENCE**
www.electrochemsci.org

# A Molecularly Imprinted Electrochemical Sensor Based on Polypyrrole/Carbon Nanotubes Composite for the Detection of S-ovalbumin in Egg White

*Qi Zeng, Xi Huang, Meihu Ma*[*]

National Research and Development Center for Egg Processing, College of Food Science and Technology, Huazhong Agricultural University, Wuhan, Hubei 430070, PR China.
[*]E-mail: mameihuhn@163.com

*Received:* 23 February 2017 / *Accepted:* 19 March 2017 / *Published:* 12 April 2017

A rapid and accurate detection of S-ovalbumin is essential for determining the freshness and quality of avian egg due to the significant correlation between them. An electrochemical sensor for S-ovalbumin detection was fabricated based on molecularly imprinted polymer (MIP) on the glass carbon electrode modified with multi-walled carbon nanotubes (MWCNTs) and chitosan (CS). The modified materials were characterized by infrared spectrometry and scanning electron microscopy. The performance of the modified electrodes, the relation between response current and analyte concentrations as well as the selectivity and practicability of MIP sensor were systematically evaluated by cyclic voltammetry, differential pulse voltammetry and electrochemical impedance spectroscopy. Under the optimum operating conditions, the fabricated electrochemical sensor showed a linear current response to the target concentration in the range from $10^{-8}$ to $10^{-4}$ mg/mL with a detection limit of $2.95\times10^{-9}$ mg/mL in S-ovalbumin detection. Additionally, the proposed sensor exhibited good selectivity, high sensitivity and desirable stability.

**Keywords:** Molecularly imprinted polymer; polypyrrole; electrochemical sensor; S-ovalbumin; egg white

## 1. INTRODUCTION

Molecular imprinting, a kind of template-assisted synthesis, assembles a complex in a 3D-polymeric network with functional monomers and template molecules. The removal of templates from the polymer exposes imprinted cavities that are complementary not only in size and shape, but also in interaction sites of template molecules [1, 2]. For these extremely interesting characteristics, molecularly imprinted polymer (MIP) is being increasingly used. A protein molecularly imprinted

electrochemical sensor is usually prepared by modifying the protein molecularly imprinted polymer on the electrode surface in the presence of functional monomers and template proteins, and the selective recognition performance of the sensor can be monitored through the changes of electrochemical signals. The sensor is promising due to its rapid response, high sensitivity, good reproducibility and low cost [3, 4]. Because of the structure variability, large molecular size and incompatibility of the protein with some functional monomers, the development of protein molecularly imprinted sensor is relatively slow [5, 6]. In recent years, however, some research progress has been achieved, such as the detection for bovine leukemia virus glycoproteins [7], bovine serum albumin[5], bovine hemoglobin[8] and human serum albumin[9]. Electropolymerization technique plays an important role in the development of electrochemical sensor, and when applied in electrochemical detection, the electroactive monomers can be precisely and homogeneously modified on the electrode surface to form a desirable polymeric film through electropolymerization [10]. Polypyrrole (Ppy) can be easily electropolymerized to immobilize different biomacromolecules for its good biocompatibility. As an excellent conductive polymer and convenient ion channel, Ppy is commonly used in electrochemical sensor development. Meanwhile, the process can directly proceed in neutral aqueous solution, which effectively maintains the natural conformation of template protein [7, 11].

Multi-walled carbon nanotubes (MWCNTs) are composed of multiple rolled layers of carbon atoms, which have large specific surface area, small particle size, high electrical conductivity and chemical stability. They have the ability to accelerate electron transfer and increase the adsorption capacity of electroactive probe on the electrode surface, then amplify the electrochemical signals [12-15]. Oxidized by concentrated acid, the MWCNTs can produce some carboxyl groups to improve hydrophilicity and interact with biomacromolecules in aqueous solution. Chitosan (CS), a natural polysaccharide biopolymer, has abundant active amino and hydroxyl groups in its molecular structure. Due to its practical physicochemical properties, such as good film-forming ability, excellent biocompatibility and high mechanical strength, CS has been widely used as immobilization matrix of nanomaterials in the field of modified electrode [16-21]. The recombination of MWCNTs and CS could overcome the drawback of MWCNTs dispersion, enabling them to be homogeneously dispersed on the electrode surface, which could increase specific surface area and enhance electrochemical signals [19]. In addition, the composite film, which has a 3D porous structure, could promote the formation of imprinted sites to interact with carboxyl and amino groups in protein through hydrogen bond, and improve the sensor specificity.

Ovalbumin, a major protein component in avian egg white, constitutes about 54% (57.24 mg/mL) of the total proteins. It is a monomeric and globular phosphorylated glycoprotein consisting of 385 amino acid residues with a molecular weight of 45 kDa [22]. During storage or hatch period, the native ovalbumin (N-ovalbumin) gradually converts into stable ovalbumin (S-ovalbumin), an irreversible and extremely heat-stable form compared with N-ovalbumin[23]. After induction in vitro, N-ovalbumin can totally convert into S-ovalbumin. The differential scanning calorimetry (DSC) and circular dichroism (CD) could be used to identify the two proteins [24, 25]. Under a certain storage temperature, as storage time increases, the S-ovalbumin content gradually rises up with the decrease of emulsifying stability as well as the foaming and gelling ability. The S-ovalbumin content in fresh egg white increases from 18.15 %(10.38 mg/mL) to 81.46 %(46.63 mg/mL) (relative to N-ovalbumin

content) after 28 days of storage at 25℃ [26]. A previous study has shown a high negative correlation of S-ovalbumin content to haugh unit and yolk index, but a high positive correlation to albumen pH [27]. Therefore, the S-ovalbumin content can be used as a reference index to evaluate the egg quality and freshness. To this end, it is necessary to develop a method for rapid and accurate detection of the S-ovalbumin content.

In this study, a sensor for the specific detection of S-ovalbumin was fabricated based on molecular imprinting and electrochemical copolymerization technology using polypyrrole, MWCNTs and CS as modified materials. In the detection process, with $[Fe(CN)_6]^{3-}$/ $[Fe(CN)_6]^{4-}$ as an electroactive probe, the target analyte bound on the imprinted sites can avoid probe diffusion through the surface of the imprinted film, leading to current decrease in a concentration-dependent manner. This principle was investigated with a systematic evaluation of the performance of different modified electrodes, the relationship between response current and analyte concentration as well as the selectivity and practicability of the sensor by using cyclic voltammetry (CV), differential pulse voltammetry (DPV) and electrochemical impedance spectroscopy (EIS).

## 2. EXPERIMENTAL

### *2.1 Reagents and apparatus*

Fresh eggs from Hy-Line Brown were collected from a local hennery (Wuhan, China). Q Sepharose Fast Flow was obtained from Beijing RuiDaHengHui Science & Technology Company (China). Multi-walled carbon nanotubes (99%, 5-15nm) was obtained from Chengdu institute of Organic Chemistry, Chinese Academy of Sciences (Chengdu, China). Polyethylene glycol 8000 (PEG-8000) (BC grade) was purchased from Shanghai Merck Chemicals Company (Shanghai, China). Pyrrole (GC grade) was purchased from Shanghai Puzhen Biotechnology Company (China). Bovine serum albumin (BSA), lysozyme (LYZ) and ovotransferrin (OVT) were purchased from the Biosharp Company (China). $HNO_3$, $H_2SO_4$, HCl, KCl, $K_3Fe(CN)_6$, $K_4Fe(CN)_6$, $Na_2HPO_4$, $KH_2PO_4$, sodium dodecyl sulfate (SDS), acetic acid, dimethylformamide (DMF) and chitosan were purchased from the Guoyao Company (China). All chemicals used were of analytical grade.

Ovalbumin was purified by chromatographic column 500 mm×16 mm using protein & nucleic acid detector (HD-3000) and constant flow pump (HL-2) (Shanghai Jiapeng Science & Technology Company, China). The modified materials were characterized by Fourier transform infrared spectrometer (FT-IR) (Nexus 470) (Mettler Company, America) and Field Emission Scanning Electron Microscopy (FE-SEM) (SU-8010) (Hitachi High-Technologies Company, Japan). Electrochemical experiments were performed using Autolab PGSTAT 204 electrochemical analysis system and Nova 1.10 software (Eco Chemie Company, Netherlands). The three-electrode system used consisted of a glass carbon electrode (GCE) (φ3mm) as the working electrode, a saturated calomel electrode as the reference electrode, and a platinum wire as the auxiliary electrode (Wuhan Gaoss Union Science & Technology Company, China).

*2.2 Preparation of S-ovalbumin*

All separation steps were carried out at 4℃. Briefly, 250 mL egg whites was stirred to uniformity for 2 h with 3 volumes of 0.5 mol/L NaCl solution. The solution pH was adjusted to 6.0 with 1 mol/L HCl, followed by the addition of 10 % PEG-8000(w/w) under magnetic stirring for 2 h. Then, the solution was centrifuged at 15000 r/min under 4℃ for 10 min, and the supernatant collected was injected to a Q Sepharose Fast Flow column which was equilibrated with 0.02 mol/L Tris-HCl buffer (pH 8.0). The flow-through fraction was eluted successively using the same buffer containing 0.08, 0.18 and 0.30 mol/L NaCl at a flow rate of 2 mL/min. The product obtained from the third peak was collected and dialyzed against distilled water 4 times. Then, the ovalbumin powder was obtained by freeze-drying and stored at -20 ℃[28].

To prepare S-ovalbumin, 2.5 g ovalbumin was dissolved in 60 mL distilled water and the solution pH was adjusted to 9.9 with 1 mol/L NaOH. After treatment at 55℃for 72 h, the solution pH was adjusted to 7.0 with 1 mol/L HCl. Finally, S-ovalbumin was obtained by dialysis and freeze-drying, and then stored at -20 ℃ [24]. The two proteins were identified by SDS-PAGE, Differential Scanning Calorimetry (DSC) and Circular Dichroism (CD) (in Figs. S1, S2 and S3, respectively).

*2.3 Preparation of CS-MWCNTs-COOH modified GCE*

The bare GCE was polished with alumina powder (0.05 μm), washed with ultrapure water, and then ultrasonicated in ethanol and ultrapure water separately for 2 min. A mirror-finished GCE obtained was immersed in a mixed solution containing 0.01 mol/L $[Fe(CN)_6]^{3-}$/ $[Fe(CN)_6]^{4-}$ and 0.1 mol/L KCl through continuous cyclic scanning between −0.20 V and 0.60 V at 100 mV/s until a characteristic cyclic voltammogram was obtained. Finally, the GCE was dried by pure nitrogen for further use.

The dispersion and stability of MWCNTs were improved by treatment with concentrated acid to introduce -COOH. Briefly, 500 mg MWCNTs and 60 mL concentrated $HNO_3$ were mixed in round-bottom flask with ultrasonic treatment for 10 min. The solution obtained was refluxed with continuous stirring at 85℃ for 72 h. Then, the solution was repeatedly washed to neutrality by ultrapure water, and the MWCNTs-COOH was obtained by vacuum drying for 12 h [19].

Ten mg MWCNTs–COOH and 10 mL CS–acetic acid solution (1.0 wt %) were mixed in a beaker under ultrasonic treatment to form a homogeneous CS-MWCNTs-COOH suspension solution (1 mg/ mL). Then, the GCE was coated with 10 μL CS-MWCNTs-COOH composite and allowed to dry at room temperature to obtain CS-MWCNTs-COOH/GCE [12]. In addition, the DMF-MWCNTs-COOH/GCE and CS/GCE were prepared for performance evaluation.

*2.4 The preparation of imprinted CS-MWCNTs-COOH/GCE*

CS-MWCNTs-COOH/GCE was immersed in a deoxygenated PBS solution (0.1 mol/L, pH 7.0) containing 0.1 mol/L pyrrole, 0.1 mol/L KCl, and 1 mg/mL S-ovalbumin. The co-polymerization was performed by CV between −0.20 V and 1.2 V at 100 mV/s for 4 cycles. After electropolymerization,

the modified GCE was immersed into 5 % acetic acid and 10 % SDS mixed solution under magnetic stirring for 1.5 h to remove S-ovalbumin, then the molecularly imprinted electrochemical sensor (MIP sensor) was obtained[29, 30]. A control electrode (NIP sensor) was prepared following the same procedure but without a template protein. The preparation process of MIP sensor is shown in Scheme 1.

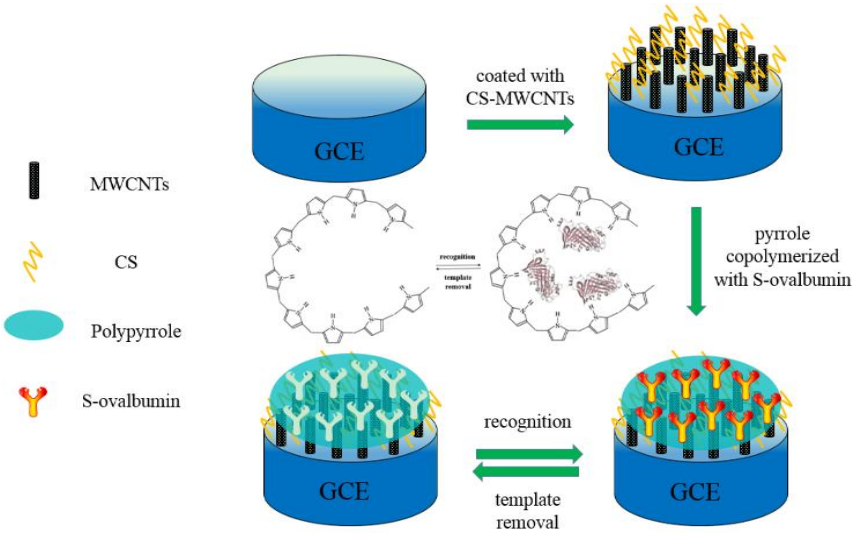


**Scheme 1.** The preparation process of MIP sensor

*2.5 FT-IR analysis*

Two mg MWCNTs-CS and MWCNTs-CS/Ppy modified materials were mixed separately with 200 mg fully dried KBr powder. The mixtures were ground homogeneously by agate mortar under the infrared lamp, and then pressed into transparent disks. The disks were scanned 32 times by FT-IR from 4000 to 400 $cm^{-1}$ at 4 $cm^{-1}$ resolution.

*2.6 Morphological characterization by FE-SEM*

The surface morphologies of bare GCE, MWCNTs-CS/GCE, S-OVA@MIP/GCE and MIP/GCE were characterized by FE-SEM.

*2.7 Electrochemical measurements*

Because of the poor electroactivity of S-ovalbumin, $[Fe(CN)_6]^{3-}$/ $[Fe(CN)_6]^{4-}$ was chosen as electroactive probe to evaluate the sensor performance. The polymer formed on the electrode surface could offer convenient channels for the transfer of probe molecules, which can cause redox reaction, and then produce electrochemical signals. When a certain amount of template proteins absorbs on the polymer surface, the channels will be blocked, which inhibits the transfer of probe molecules and weakens the electrochemical signals. Therefore, all the electrochemical measurements were carried out in a PBS solution containing 0.01 mol/L $[Fe(CN)_6]^{3-}$/ $[Fe(CN)_6]^{4-}$and 0.1 mol/L KCl. The CV was

used to measure the performance of different modified GCE and investigate the relation between scan rate and peak current. Then DPV and EIS were used to make a comparison between MIP sensor and NIP sensor and investigate the dependent relation between the concentration of S-ovalbumin and peak current. Additionally, BSA (66.4 kDa), LYZ (14.3 kDa) and OVT (76.7 kDa) were used as interfering substances to evaluate the selectivity of the MIP sensor.

### *2.8 Application of the MIP sensor*

To begin with, 25 ng/mL, 50 ng/mL and 75 ng/mL S-ovalbumin standard solutions were prepared. Then the proposed MIP sensor was used to detect these three standard solutions by DPV for the purpose of confirming the accuracy. The determined concentrations of S-ovalbumin were obtained through substituting the peak current into the linear equation (shown in subtitle 3.4). Subsequently, the recovery was calculated by standard concentration and determined concentration of S-ovalbumin. In addition, for the real samples, 10 mL egg whites were stirred for 5 min and heated at 55℃ for 30 min, followed by centrifugation at 12000 r/min for 5 min. One mL diluted supernatant was mixed with 9 mL PBS (0.1 mol/L, pH 7.0) solution containing 0.01 mol/L $[Fe(CN)_6]^{3-}$/ $[Fe(CN)_6]^{4-}$ and 0.1 mol/L KCl, then the measurement was carried out.

## 3. RESULTS AND DISCUSSION

### *3.1 FT-IR analysis*

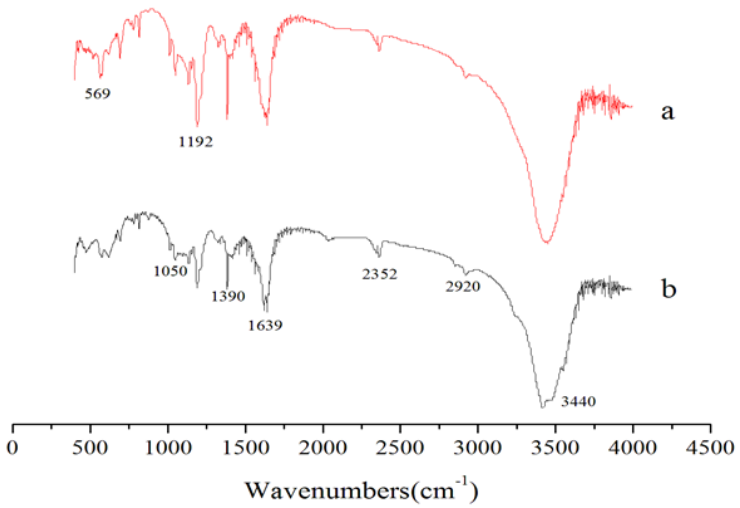


**Figure 1.** Infrared spectra of (a) MWCNTs-CS/Ppy and (b) MWCNTs-CS.

The infrared spectra of MWCNTs-CS/Ppy and MWCNTs-CS are shown in Fig.1. As shown in Fig.1b, after treatment with concentrated acid, MWCNTs can produce some carboxyl groups and absorb carbon dioxide, giving rise to two peaks at 1639 $cm^{-1}$ (stretching vibration of -C=O in carboxyl

groups) and 2352 $cm^{-1}$ (stretching vibration of O=C=O)[31, 32]. The molecular structure of chitosan has a large number of -$NH_2$, -OH, -C-O-C- and -$CH_2$ groups, with the related peaks at 3440 $cm^{-1}$(a overlapping peak for the stretching vibration of -$NH_2$ and -OH), 1050 $cm^{-1}$(the stretching vibration of -C-O-C-), 1390 $cm^{-1}$(the stretching vibration of -$CH_2$-) and 2920 $cm^{-1}$(the stretching vibration of -C-H), respectively.[31, 33]. It can be seen from Fig.1a that the molecular structure of polypyrrole contains -CH-NH-CH- and -CH=CH-, with the related peaks at 1192 $cm^{-1}$(the bending vibration of -CH-NH-CH-) and 569 $cm^{-1}$(the trans olefin skeleton vibration of -CH=CH-). The results indicated that polypyrrole was successfully deposited on the surface of MWCNTs-CS film.

### *3.2 Morphological characterization by FE-SEM*

The SEM can be used to visually observe the morphologies of different modified electrodes. Fig.2A represents the morphology of bare GCE. It can be seen that the GCE surface is flat and smooth after polishing and washing. In Fig.2B, it is clearly observed that MWCNTs were distributed on the surface or inserted in the chitosan film after modification on the GCE surface.

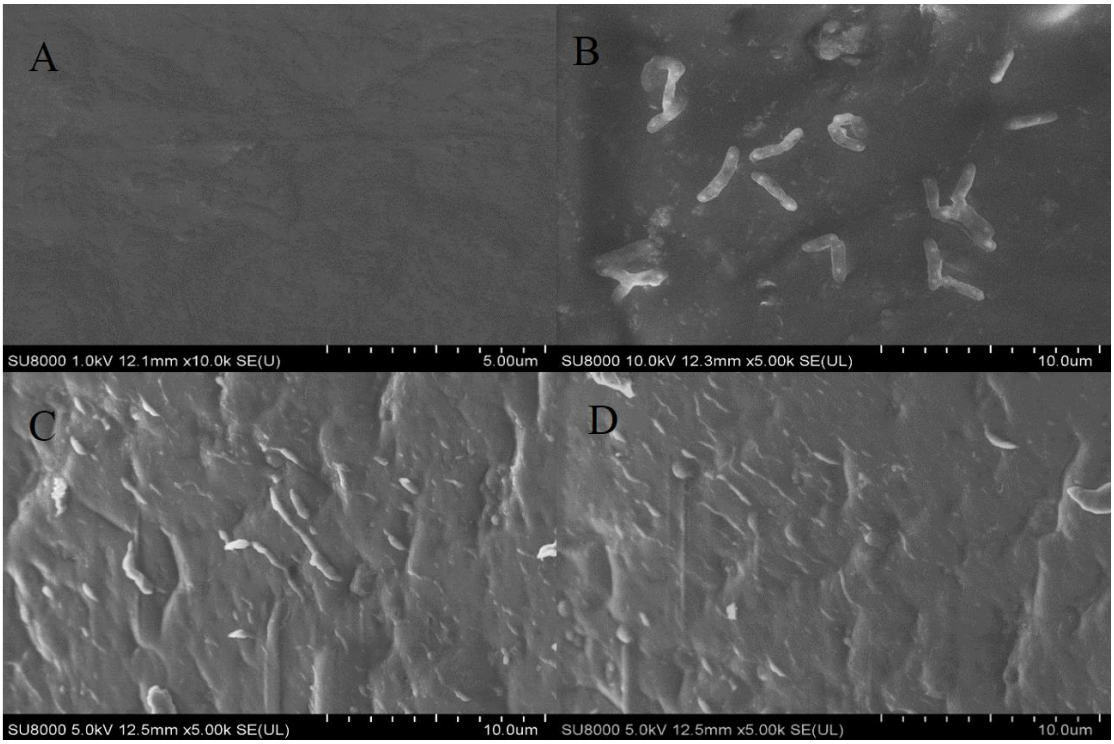


**Figure 2.** SEM images of (A) bare GCE, (B) MWCNTs-CS/GCE, (C)MWCNTs-CS/S-OVA@MIP/GCE and (D) MWCNTs-CS/MIP/GCE.

However, in Fig.2C, the surface of GCE is rough and uneven, with some small particles deposited on the MWCNTs, indicating that polypyrrole was successfully modified on the GCE surface. The morphology of the imprinted GCE with elution step is represented in Fig.2D. When compared

with Fig.2C, the GCE morphology had no significant change, which was similar to the previous studies[34, 35].

### *3.3 Characterization of electrochemical performance*

Generally, the electrochemical mechanism on the electrode surface can be acquired from the relation between peak current and scan rate [36]. Fig.3A shows the cyclic voltammogram of MWCNTs-CS/GCE at the scan rate from 50 mV/s to 150 mV/s. It can be observed that the redox peak current gradually increased with the increase of scan rate. Fig.3B represents the curves of peak current versus scan rate. As shown in the figure, both the anodic ($I_{pa}$) and cathodic ($I_{pc}$) peak currents were linearly related to the square root of scan rate, with the linear regression equations $I_{pa}$(mA) = 0.0022+0.0347 $V^{1/2}$(mV/s)($R^2$ =0.9998) and $I_{pc}$(mA) = -0.0396-0.0271$V^{1/2}$(mV/s)($R^2$ =0.9997).

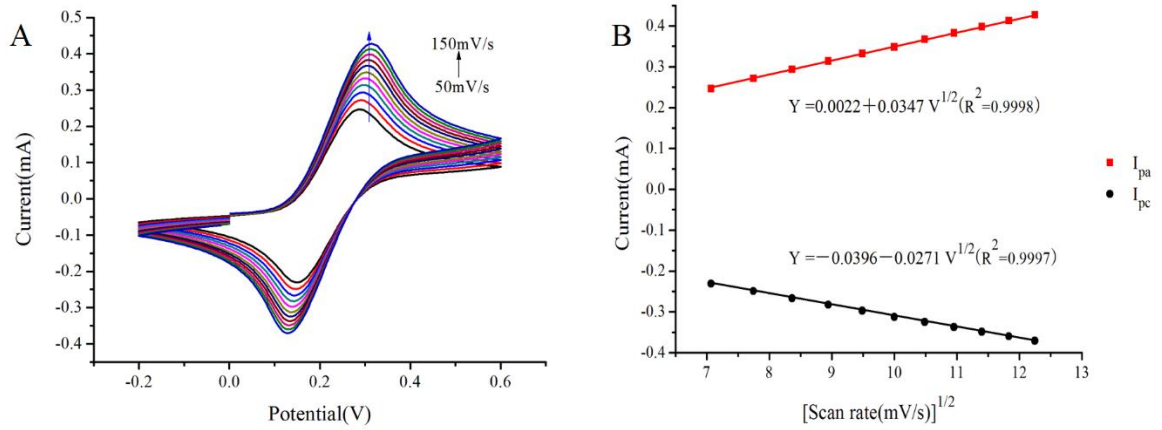


**Figure 3.** (A) CV for MWCNTs-CS/GCE in a 0.01 mol/L $Fe(CN)_6^{3-/4-}$ and 0.1 mol/L KCl solution (scan rate: 50 to 150 mV/s, scan range: -0.2 to 0.6 V). (B) peak current curves, Ipa and Ipc.

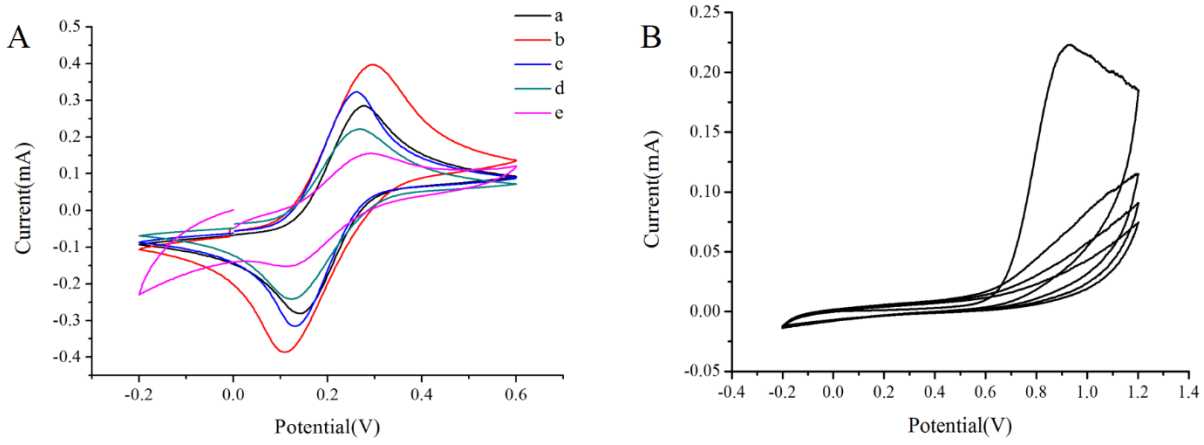


**Figure 4.** (A) CV for (a) bare-GCE, (b) MWCNTs-CS/GCE, (c) MWCNTs /GCE, (d) CS /GCE and (e) S-OVA@MIP/GCE in a 0.01 mol/L $Fe(CN)_6^{3-/4-}$ and 0.1 mol/L KCl solution. (B) CV for MWCNTs-CS/GCE electropolymerized in a 0.1 mol/L pyrrole, 1 mg/mL S-ovalbumin and 0.1 mol/L KCl solution.

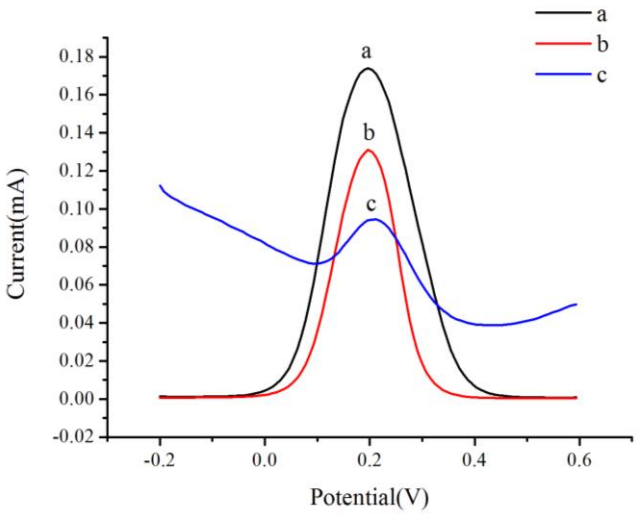


**Figure 5.** DPV for (a) MWCNTs-CS/GCE, (b) bare-GCE and (c) S-OVA@MIP/GCE in a 0.01 mol /L $Fe(CN)_6^{3-/4-}$ and 0.1 mol/L KCl solution.

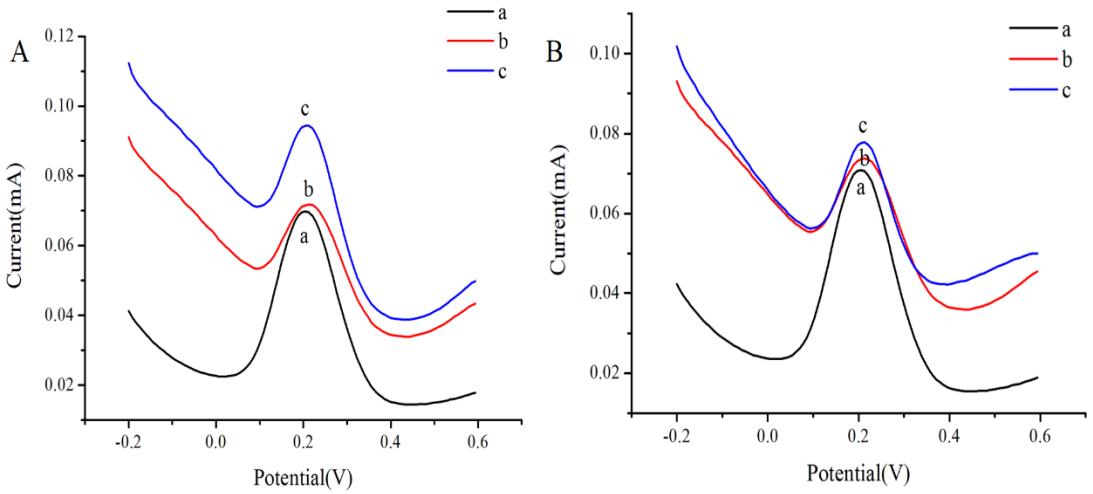


**Figure 6.** DPV for (A) MIP sensor and (B) NIP sensor, the sensor (a) before and (c) after elution in a 5 % acetic acid and 10 % SDS solution, followed by (b) incubation in a $10^{-3}$ mg/mL S-ovalbumin solution containing 0.01 mol /L $Fe(CN)_6^{3-/4-}$ and 0.1 mol/L KCl for 40 min.

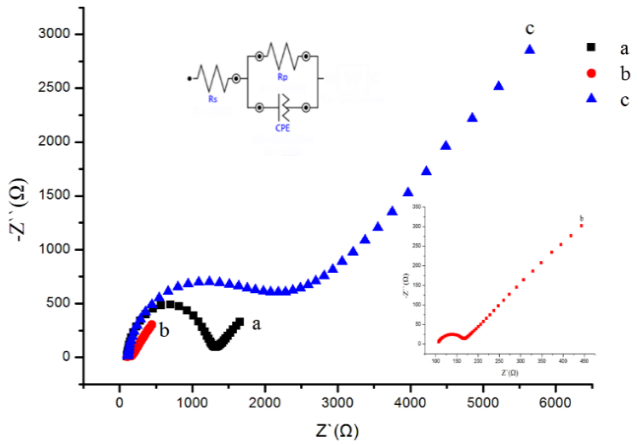


**Figure 7.** EIS for (a) bare-GCE, (b) MWCNTs-CS/GCE and (c) S-OVA@MIP/GCE in 0.01 mol/L $Fe(CN)_6^{3-/4-}$ and 0.1 mol/L KCl solution. Inset: Equivalent electrical circuit diagrams. Rp: electron transfer resistance, Rs: electrolyte resistance, CPE: constant phase element.

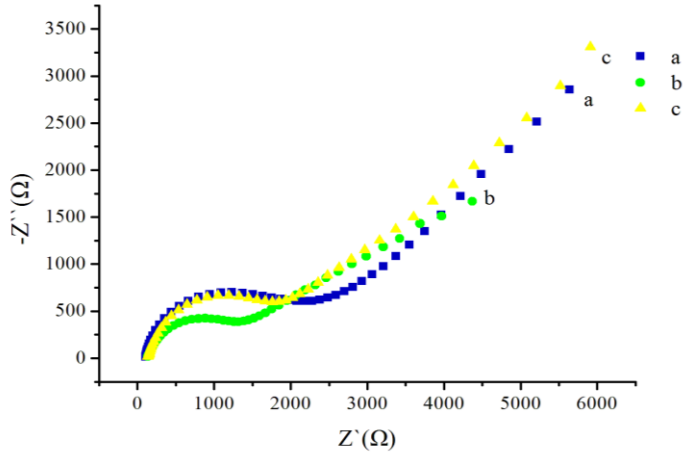


**Figure 8.** EIS for MIP sensor (a) before and (c) after elution in a 5 % acetic acid and 10 % SDS solution, followed by (b) incubation in a $10^{-3}$ mg/mL S-ovalbumin solution containing 0.01 mol /L $Fe(CN)_6^{3-/4-}$ and 0.1 mol/L KCl for 40 min.

The results demonstrated that the reaction process on the electrode surface was predominantly diffusion-controlled, suggesting that MWCNTs-CS played an important role in enhancing the electron-transfer rate [32, 37].

CV is an effective method for monitoring the electron transfer process of modified electrode surface. As shown in Fig.4A (a), the bare GCE exhibited a couple of redox peaks. After the GCE modification with chitosan (Fig.4A (d)), due to its relatively poor conductivity, the chitosan film increased the resistance of GCE surface, resulting in the decrease of peak current and the reaction reversibility [18, 33]. When the GCE was modified with MWCNTs-CS composite film (Fig.4A (b)), the redox peak current increased significantly, which can be attributed to the reason that MWCNTs were homogenously dispersed on the GCE surface with the assistance of chitosan, thus expanding the electroactive area, increasing the absorption capacity of electroactive probe, and finally enhancing the response current [33, 36]. When the GCE was only modified with MWCNTs (Fig.4A (c)), the response current had no significant increase due to the poor dispersibility of MWCNTs. When the MWCNTs-CS/GCE was modified with the imprinted film (Fig.4A (e)), the response current decreased significantly in the presence of S-ovalbumin [38]. Fig.4B represents the cyclic voltammogram of preparing S-OVA@MIP/GCE by electropolymerization. The MIP film was deposited by repeatedly scanning from -0.2 V to 1.2 V at 100 mV/s for 4 cycles. During the first cycle, an oxidation peak clearly observed at 0.9 V was possibly assigned to the polymerization reaction of pyrrole, indicating the formation of a compact polymeric film on the GCE surface. The current decreased with the increase of scan cycle, which was related to the continuous formation of polypyrrole doped with S-ovalbumin. Additionally, the optimization of scan rate, removal time and incubation time is shown in Figs. S4, S5 and S6, respectively.

DPV is an electrochemical measurement technique with high detection sensitivity and often used to analyze the electrochemical performance of different modified electrodes. As shown in Fig.5b, the bare GCE displayed an obvious oxidation peak at 0.2 V. The modification of MWCNTs-CS composite on the GCE surface (Fig.5a) improved the electrochemical reactive activity and then

enhanced the peak current ($\Delta I_p \approx 0.045$ mA). After further deposition with imprinted film (Fig.5c), the conductivity of modified GCE weakened and then peak current decreased significantly ($\Delta I_p \approx 0.08$ mA). The results above are in accordance with CV.

In order to evaluate the validity of imprinting performance of MIP sensor, DPV was used to make a comparison between MIP and NIP sensor, including before and after the elution as well as incubation in the $10^{-3}$ mg/ml S-ovalbumin solution. As shown in Fig.6A, when the MIP sensor was eluted (Fig.6A(c)), the peak current increased dramatically ($\Delta Ip \approx 0.027$ mA) compared with that before elution (Fig.6A (a)). This was attributed to the formation of some imprinted sites and caves on the polymer surface after template elution, which offered convenient channels for the transfer of the probe molecules, and increased the electron transfer number of GCE surface. Since the surface of the eluted MIP sensor contains some active groups and imprinted caves that can match with the conformation and size of S-ovalbumin, when it was incubated in the $10^{-3}$ mg/ml S-ovalbumin solution (Fig.6A (b)), the S-ovalbumin would attach to the surface of MIP sensor and block the imprinted caves, leading to a notable decrease of the peak current ($\Delta Ip \approx 0.025$ mA). As shown in Fig.6B, when the NIP sensor was eluted (Fig.6B(c)), the peak current increased in a certain extent ($\Delta Ip \approx 0.0075$ mA). When the eluted NIP sensor was incubated in the S-ovalbumin solution (Fig.6B (b)), the peak current decreased slightly ($\Delta I_p \approx 0.004$ mA). The results were attributed to the microstructure change of NIP sensor after elution and the existence of non-specific binding. Therefore, when compared with NIP sensor, MIP sensor has good imprinting performance and could be used for S-ovalbumin detection.

EIS is an effective technique for monitoring the interface properties of modified electrodes. Generally, the impedance spectrum includes a semicircle part and a linear part. The linear part at lower frequencies corresponds to the diffusion process, while the semicircle diameter at higher frequencies is equivalent to the electron-transfer resistance ($R_{et}$) that reveals the electron-transfer kinetics of the redox probe and could be estimated by using the equivalent circuit as shown by the inset in Fig.7 [39-41]. In Fig.7a, the bare GCE displayed a typical impedance spectrum, with the Ret estimated to be 1160 Ω. After the bare GCE was modified with MWCNTs-CS composite (Fig.7b), the resistance for the redox probe significantly decreased ($R_{et}$=59.5 Ω), suggesting that MWCNTs-CS composite is an excellent conducting material and could accelerate the electron transfer. After further modification with imprinted film (Fig.7c), the resistance dramatically increased ($R_{et}$=1980 Ω), indicating that the modified layer formed an additional barrier and then hindered the redox probe to the GCE surface. It can be observed from Fig.8 that, after elution (Fig.8b), the resistance on the surface of MIP sensor decreased due to the removal of template protein ($R_{et}$=1400 Ω). After further incubation in the S-ovalbumin solution (Fig.8c), the resistance increased for the absorption of S-ovalbumin on the MIP sensor ($R_{et}$=1720 Ω). Therefore, the EIS results further confirmed the DPV results.

### *3.4 Electrochemical detection of S-ovalbumin*

In the process of electrochemical measurement, the DPV exhibits high sensitivity and low detection limit due to the deduction of background current, and thus has been widely applied in quantitative analysis[42]. Fig.9A shows the differential pulse voltammograms of the MIP sensor in the

S-ovalbumin concentration range of $10^{-8}$ mg/mL to $10^{-2}$ mg/mL in PBS containing $[Fe(CN)_6]^{3-}/[Fe(CN)_6]^{4-}$. It is observed that the peak current decreased with the increase of S-ovalbumin concentration, suggesting a negative correlation between them. But for the high concentrations, the current signals remained stable owing to the saturation between S-ovalbumin molecules and the binding sites on the MIP sensor. As shown in Fig.9B, there is a good linear relation between S-ovalbumin concentration and peak current from $10^{-8}$ mg/mL to $10^{-4}$ mg/mL (Ip (mA) = 0.0048－0.0034log [Cs-ova] ($R^2$ =0.998)), and the detection limit of MIP sensor is $2.95\times10^{-9}$ mg/mL (S/N=3).The results for the other similar molecularly imprinted electrochemical sensors are summarized in Table 2. On the whole, the linear range or detection limit of our sensor compares well with those reported in the literature.

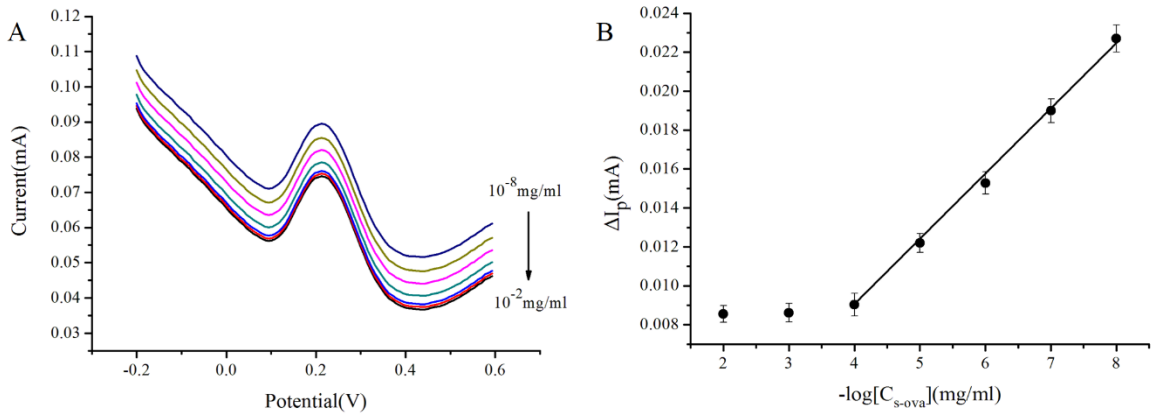


**Figure 9.** (A) DPV of MIP sensor incubated for 40 min in a solution containing 0.01 mol /L Fe (CN)$_6^{3-/4-}$ and 0.1 mol/L KCl with different concentrations of S-ovalbumin. (B) Calibration curve of peak current versus S-ovalbumin concentration (from $10^{-8}$ mg/mL to $10^{-2}$ mg/mL)

*3.5 Selectivity measurement*

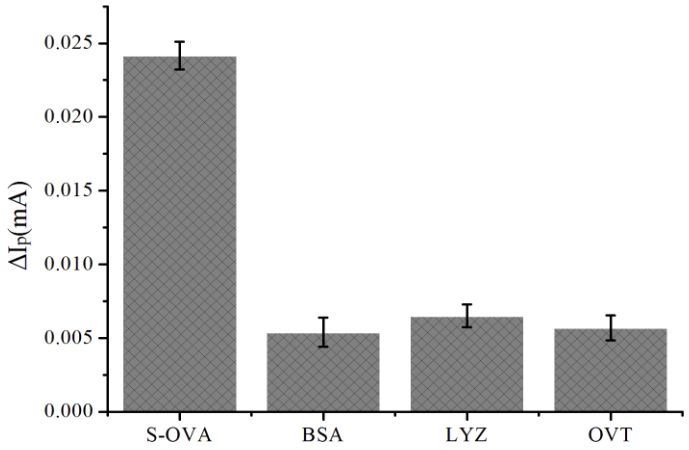


**Figure 10.** The selectivity of MIP sensor for $10^{-3}$ mg/mL S-ovalbumin, BSA, LYZ and OVT

Non-electroactive protein could absorb on the surface of MIP sensor by interacting with imprinted sites, and thus weaken the response current. To explore this principle, BSA, LYZ and OVT were chosen as interfering substances to evaluate the selectivity capacity of MIP sensor by DPV. As shown in Fig.10, the changes of response current caused by BSA, LYZ and OVT were 0.0054 mA, 0.0065 mA and 0.0057 mA, respectively, while the current change of S-ovalbumin was 0.0242 mA, which is much higher than any of the former three proteins. Generally, in view of the specific structure of imprinted film, the template protein could enter imprinted sites properly, leading to low diffusion of probe and weak current, but it was not the case for the other proteins [5]. The current decrease for the other proteins was mainly attributed to non-specific binding of the MIP sensor (such as the effects of carboxyl, hydroxyl and amine groups).

### *3.6 Reproducibility, stability and applicability of the MIP sensor*

After washing three times, the MIP sensor showed good reproducibility with a relative standard deviation of 7.24 %. As a key factor for analyte detection, the stability of MIP sensor was evaluated. The MIP sensor was stored in PBS (0.1 mol/L, pH 7.0) at 4℃ for 15 days, the peak current decreased to 92.18 %. To identify the applicability of the proposed sensor, the S-ovalbumin content in standard solutions was detected using the standard recovery method mentioned in subtitle 2.8. The results in Table 1 indicated that MIP sensor exhibited good recoveries at three levels, implicating the accurate quantification of S-ovalbumin. Besides, according to the experiment procedure, the concentration of S-ovalbumin determined in fresh egg whites was 10.303 mg/mL.

**Table 1.** Results of the recovery experiment in standard solution

| Sample | Concentration of S-ovalbumin (ng/mL) | Determined concentration of S-ovalbumin (ng/mL) | Recovery (%) | RSD(%)(n=3) |
|---|---|---|---|---|
| 1 | 25 | 23.05 | 92.2 | 3.75 |
| 2 | 50 | 47.83 | 95.66 | 4.11 |
| 3 | 75 | 71.21 | 94.95 | 2.77 |

**Table 2.** Comparison with the other similar molecularly imprinted electrochemical sensors

| Electrode used | Technique | Linear range | Detection limit | Analyte | Reference |
|---|---|---|---|---|---|
| Ppy/MNPs/CS-MWCNTs/GCE | DPV | $10^{-7}$-$10^{-1}$ mg/mL | $2.8\times10^{-8}$ mg/mL | Bovine serum albumin | [43] |
| CS/ionic liquid-graphene/GCE | DPV | $10^{-10}$-$10^{-4}$ mg/mL | $2\times10^{-11}$ mg/mL | Bovine serum albumin | [30] |
| Ppy/AuE | DPV | $10^{-9}$-$10^{-3}$ mg/mL | no | Bovine hemoglobin | [44] |

| | | | | | |
|---|---|---|---|---|---|
| Ppy/MWCNTs/GCE | DPV | $6.25\times10^{-7}$-$1.0\times10^{-4}$ mol/L | $6\times10^{-8}$ mol/L | dopamine | [45] |
| Sol-gol/CS-MWCNTs/GCE | DPV | $2.0\times10^{-6}$-$1.0\times10^{-3}$ mol /L | $4.4\times10^{-7}$ mol /L | Quinoxaline-2-carboxylic acid | [19] |
| Ppy/CS-MWCNTs/GCE | DPV | $10^{-8}$ - $10^{-4}$ mg/mL | $2.95\times10^{-9}$ mg/mL | S-ovalbumin | This work |

## 4. CONCLUSIONS

In summary, an electrochemical imprinted sensor for S-ovalbumin detection was successfully prepared by electropolymerizing MIP film onto MWCNTs-CS composite modified GCE and characterized by several methods. The fabricated MIP sensor exhibited favorable performance with a low detection limit, good stability and desirable applicability. The present method may have the potential application for evaluation of the freshness and quality of avian eggs. However, an in-depth study is also needed for further improving the performance of MIP sensor by eliminating non-specific interactions and increasing the reusability.

*SUPPLEMENTARY MATERIAL:*

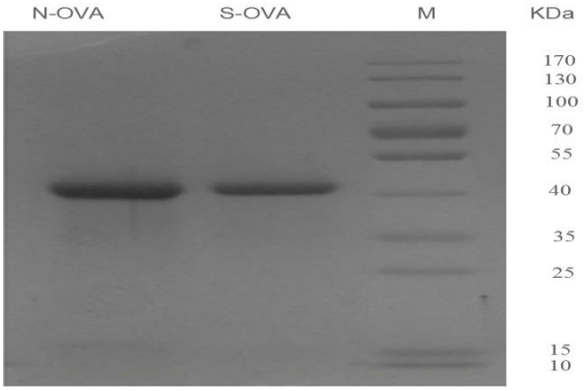


**Fig. S1** SDS-PAGE profile of ovalbumin

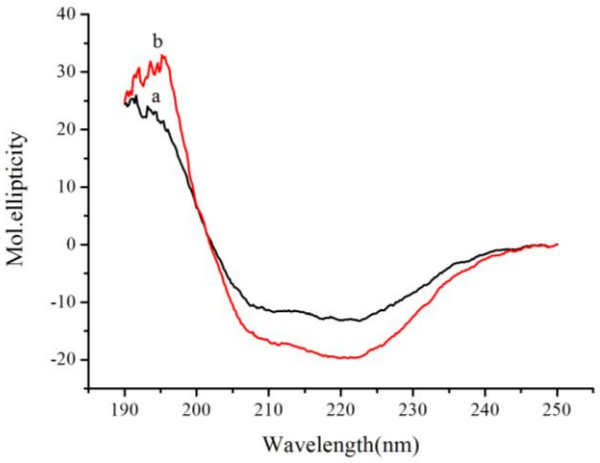


**Fig. S2** CD profile of ovalbumin after 0 h (a) and 72 h (b) induction

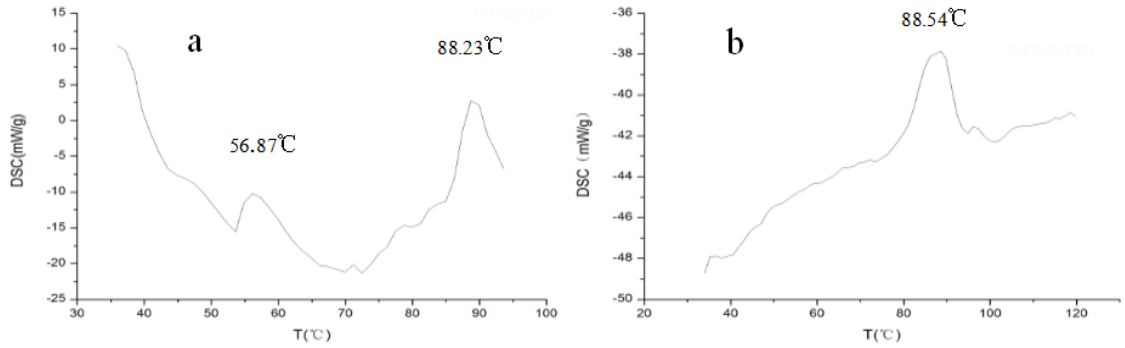


**Fig. S3** DSC profiles of ovalbumin after 0 h (a) and 72 h (b) induction

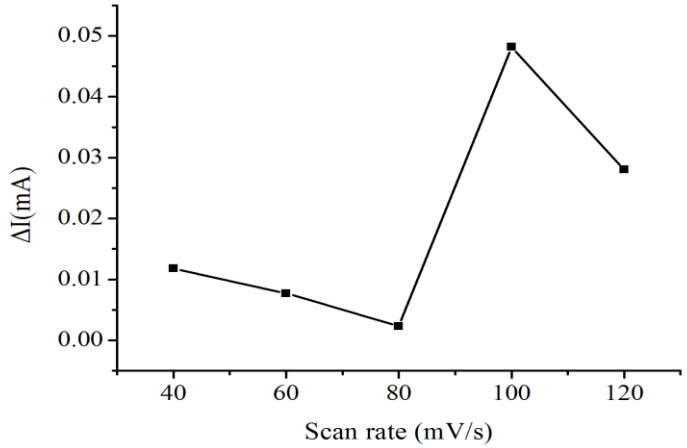


**Fig. S4** The effect of electropolymerization scan rate on current changes

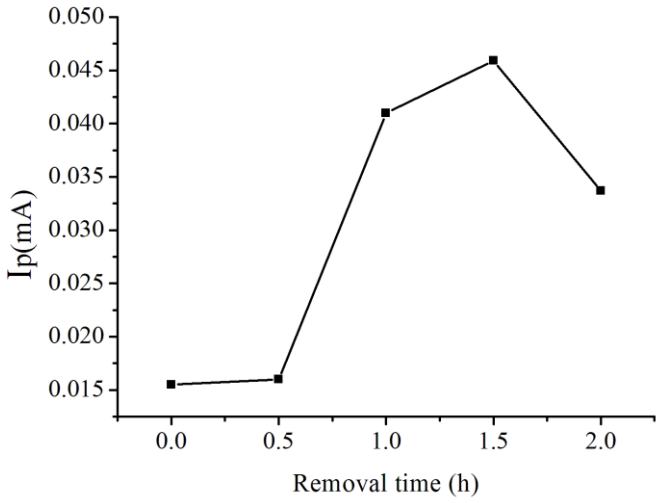


**Fig. S5** The optimization of removal time for template protein

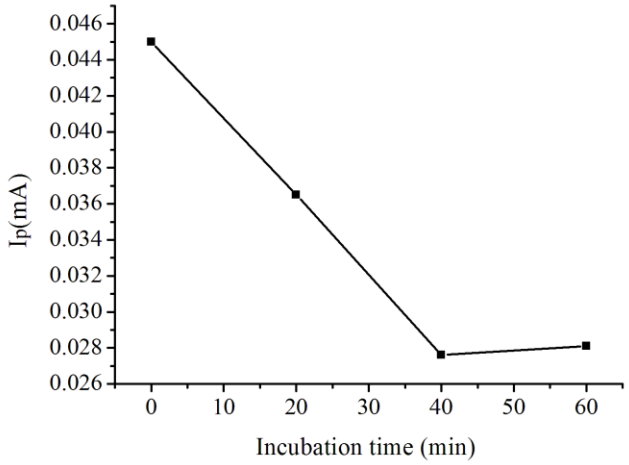


**Fig. S6** The optimization of incubation time

ACKNOWLEDGMENTS
This research was supported by National Natural Science Foundation (Project code No. 31571784).

## References

1. K. Haupt and K. Mosbach, *Chemical Reviews*, 100(2000) 2495.
2. L. Uzun and A. Turner, *Biosens. Bioelectron.*, 76(2016) 131.
3. V. Suryanarayanan, C. Wu, and K. Ho, *Electroanalysis*, 22(2010) 1795.
4. S. Wu, W. Tan, and H. Xu, *Analyst*, 135(2010) 2523.
5. H. Chen, Z. Zhang, L. Luo, and S. Yao, *Sensors and Actuators B: Chemical*, 163(2012) 76.
6. E. Verheyen, J. Schillemans, M. van Wijk, M. Demeniex, W. Hennink, and C. van Nostrum, *Biomaterials*, 32(2011) 3008.
7. A. Ramanaviciene and A. Ramanavicius, *Biosens. Bioelectron.*, 20(2004) 1076.
8. Z. Wang, F. Li, J. Xia, L. Xia, F. Zhang, S. Bi, G. Shi, Y. Xia, J. Liu, Y. Li, and L. Xia, *Biosens. Bioelectron.*, 61(2014) 391.
9. M. Cieplak, K. Szwabinska, M. Sosnowska, B. Chandra, P. Borowicz, K. Noworyta, F. D'Souza, and W. Kutner, *Biosens. Bioelectron.*, 74(2015) 960.
10. J. Deng, S. Ju, Y. Liu, N. Xiao, J. Xie, and H. Zhao, *Food Analytical Methods*, 8(2015) 2437.
11. A. Ramanavičius, A. Malinauskas, A., *Electrochimica Acta*, 51(2006) 6025.
12. J. Ji, Z. Zhou, X. Zhao, J. Sun, and X. Sun, *Biosens. Bioelectron.*, 66(2015) 590.
13. W. Tang, W. Li, Y. Li, M. Zhang, and X. Zeng, *New J. Chem.*, 39(2015) 8454.
14. Y. Tsai, S. Li, and S. Liao, *Biosens. Bioelectron.*, 22(2006) 495.
15. S. Park, H. Kang, Y. Kim, D. Lee, and C. Jin, *Bulletin of the Korean Chemical Society*, 37(2016) 174.
16. X. Ding, Y. Wang, Y. Wang, Q. Pan, J. Chen, Y. Huang, and K. Xu, *Anal. Chim. Acta*, 861(2015) 36.
17. L. Wang, W. Wen, H. Xiong, X. Zhang, H. Gu, and S. Wang, *Anal. Chim. Acta*, 758(2013) 66.
18. Y. Wen, W. Wen, X. Zhang, and S. Wang, *Biosens. Bioelectron.*, 79(2016) 894.
19. Y. Yang, G. Fang, G. Liu, M. Pan, X. Wang, L. Kong, X. He, and S. Wang, *Biosens. Bioelectron.*, 47(2013) 475.
20. C. Zhang, X. Jia, Y. Wang, M. Zhang, S. Yang, and J. Guo, *J .Sep. Sci.*, 37(2014) 419.

21. H. Kim and U. Shin, *Bulletin of the Korean Chemical Society*, 37(2016) 500.
22. M. Yamasaki, N. Takahashi, and M. Hirose, *J. Biol. Chem*., 278(2003) 35524.
23. M. Smith and J. Back, *Australian journal of biological sciences*, 18(1965) 365.
24. J. Groot, H. Kosters, and H. Jongh, *Biotechnol .Bioeng*., 97(2007) 735.
25. J. Donovan and C. Mapes, *J. Sci. Fd Agric*., 27(1976) 197.
26. A. Alleoni and A. Antunes, *Revista Brasileira de Ciência Avícola*, 6(2004) 105.
27. Q. Huang, N. Qiu, M. Ma, Y. Jin, H. Yang, F. Geng, and S. Sun, *Poult. Sci*., 91(2012) 739.
28. F. Geng, Q. Huang, X. Wu, G. Ren, Y. Shan, G. Jin, and M.H. Ma, *Separation and Purification Technology*, 96(2012) 75.
29. D. Cai, L. Ren, H. Zhao, C. Xu, L. Zhang, Y. Yu, H. Wang, Y. Lan, M. Roberts, and J. Chuang, *Nature nanotechnology*, 5(2010) 597.
30. J. Xia, X. Cao, Z. Wang, M. Yang, F. Zhang, B. Lu, F. Li, L. Xia, Y. Li, and Y. Xia, *Sensors and Actuators B: Chemical*, 225(2016) 305.
31. S. Pati, L. Singh, E. Guimarães, J. Mantilla, J. Coaquira, A. Oliveira, V. Sharma, and V. Garg, *Journal of Alloys and Compounds*, 684(2016) 68.
32. N. Sahoo, Y. Jung, H. So, and J. Cho, *Synthetic Metals*, 157(2007) 374.
33. C. Fan, K. Li, Y. Wang, X. Qian, and J. Jia, *RSC Adv*., 6(2016) 2678.
34. R. Ouyang, J. Lei, H. Ju, and Y. Xue, *Advanced Functional Materials*, 17(2007) 3223.
35. X. Wei, X. Li, and S. Husson, *Biomacromolecules*, 6(2005) 1113.
36. Y. Hu, J. Li, Z. Zhang, H. Zhang, L. Luo, and S. Yao, *Anal. Chim. Acta*, 698(2011) 61.
37. F. Li, J. Song, C. Shan, D. Gao, X. Xu, and L. Niu, *Biosens. Bioelectron*., 25(2010) 1408.
38. L. Ozcan and Y. Şahin, *Sensors and Actuators B: Chemical*, 127(2007) 362.
39. Y. Hu, Z. Zhang, J. Li, H. Zhang, L. Luo, and S. Yao, *Biosens. Bioelectron.*, 31(2012) 190.
40. E. Katz and I. Willner, *Electroanalysis*, 15(2003) 913.
41. J. Qiu, H. Peng, R. Liang, and X. Xia, *Biosens. Bioelectron*., 25(2010) 1447.
42. M. Majidi, R. Fadakar Bajeh Baj, and A. Naseri, *Food Analytical Methods*, 6(2012) 1388.
43. H. Chen, Z. Zhang, L. Luo, and S. Yao, *Sensors & Actuators B Chemical*, 163(2012) 76-83.
44. X. Kan, Z. Xing, A. Zhu, Z. Zhao, G. Xu, C. Li, and H. Zhou, *Sensors and Actuators B: Chemical*, 168(2012) 395-401.
45. X. Kan, H. Zhou, C. Li, A. Zhu, Z. Xing, and Z. Zhao, *Electrochimica Acta*, 63(2012) 69-75.